PHYSICS

Deterministic storage and retrieval of telecom light from a quantum dot single-photon source interfaced with an atomic quantum memory

Sarah E. Thomas[1]†, Lukas Wagner[2]†, Raphael Joos[2], Robert Sittig[2], Cornelius Nawrath[2], Paul Burdekin[1], Ilse Maillette de Buy Wenniger[1], Mikhael J. Rasiah[1], Tobias Huber-Loyola[3], Steven Sagona-Stophel[1], Sven Höfling[3], Michael Jetter[2], Peter Michler[2], Ian A. Walmsley[1], Simone L. Portalupi[2], Patrick M. Ledingham[4]*

A hybrid interface of solid-state single-photon sources and atomic quantum memories is a long sought-after goal in photonic quantum technologies. Here, we demonstrate deterministic storage and retrieval of light from a semiconductor quantum dot in an atomic ensemble quantum memory at telecommunications wavelengths. We store single photons from an indium arsenide quantum dot in a high-bandwidth rubidium vapor–based quantum memory, with a total internal memory efficiency of (12.9 ± 0.4)%. The signal-to-noise ratio of the retrieved light field is 18.2 ± 0.6, limited only by detector dark counts.

INTRODUCTION

Atomic ensembles are a powerful platform used to couple light to atomic degrees of freedom (*1*), playing a key role as processing nodes for quantum information protocols. Depending on the protocol, these nodes are required to store and recall (*2*), convert the frequency (*3*) and bandwidth (*4*), distill (*5*), or filter (*4*, *6*) incoming photonic quantum states. A promising platform to deliver two useful classes of photonic quantum states are semiconductor quantum dots (QDs), emerging as high-performing on-demand sources of single (*7*, *8*) and entangled photon pairs (*9*) at high operational repetition rates. QD sources of these states are typically several orders of magnitude brighter than heralded single photons or photon pairs from sources based on nonlinear spontaneous scattering. An important task therefore is to efficiently interface QDs and atomic ensembles as a first step toward hybrid light-matter interfacing and processing.

To build scalable quantum networks, it is necessary to operate at telecommunication-band wavelengths to exploit extensive existing telecom infrastructure of low-loss, cheap, and reliable optical components and direct connectivity with commercial deployed fiber networks. One possible route is to use QD sources at other wavelengths such as those at 780 nm (*10*) or 925 nm (*7*) and then use quantum frequency conversion to telecommunication wavelengths (*11*, *12*). However, the efficiency of quantum frequency conversion is not unity, can introduce noise, and requires additional experimental overheads. Alternatively, it is possible to use QD sources and quantum memories that operate directly at telecommunication wavelengths. Storing and actively recalling telecom QD light from an atomic ensemble quantum memory constitute a pivotal first step in any hybrid quantum networking approach.

Achieving an efficient light-matter interface between single photons and a quantum memory requires matching both the central wavelength and the bandwidth between the systems. Parametric down-conversion sources can generate heralded single photons with wavelengths compatible with quantum memories by means of choosing the appropriate choice of pump and quasi-phase matching, providing stable and terahertz-wide photons that can be filtered (*13*, *14*) or cavity-enhanced (*15*, *16*) to achieve highly effective matching to memories with megahertz-gigahertz bandwidth. In contrast, it is much more challenging to match both the emission wavelength and bandwidth of QD light to atomic quantum memories. Substantial advancements have been made to design and fabricate QDs that emit light with wavelengths close to atomic transitions with a typical spread of several-nanometer fine-tuning of the emitted wavelength that can then be achieved through the application of external electric (*17*) or magnetic fields (*18*), strain via piezoelectric actuators (*19*–*21*), or by temperature (*22*). The next challenge arises from matching the quantum memory bandwidth to that of the QD emission. QDs emit photons with bandwidth on the order of a few gigahertz, but environmental effects such as strain, charge noise, and spin noise can cause emission wavelength inhomogeneities of order terahertz (*23*) and temporal instability such as blinking. Many of the leading memories are incompatible, having storage bandwidths in the near megahertz regime (*24*–*26*). A promising approach is to use two-photon absorption mechanisms in hot alkali vapors. Electromagnetically induced transparency (*16*, *27*) and the fast ladder memory (*28*) have pushed the operational bandwidth to the near-gigahertz regime. The Raman (*29*) and off-resonant cascaded absorption (ORCA) memories have achieved bandwidths of 1 GHz (*6*, *14*). Last, it is key that the memory does not introduce noise so that the quantum character of the input state of light in unchanged upon retrieval.

While challenging, there has been considerable progress toward interfacing QD photons with atomic systems. Light from QDs has been shown to interact with hot rubidium (*18*, *30*) and cesium vapor (*31*–*36*) showing slow- and fast-light effects, or dispersion-induced delay, at near-infrared wavelengths. Further, the temporal intensity profile of QD photons has been observed to be modified by fast electromagnetically induced transparency in a hot rubidium cell (*37*). Direct coupling of 935-nm QD light with a trapped Yb^+ ion

[1]Department of Physics, Imperial College London, London SW7 2BW, UK. [2]Institut für Halbleiteroptik und Funktionelle Grenzflächen (IHFG), Center for Integrated Quantum Science and Technology (IQ^{ST}) and SCoPE, University of Stuttgart, Allmandring 3, 70569 Stuttgart, Germany. [3]Julius-Maximilians-Universität Würzburg, Physikalisches Institut and Würzburg-Dresden Cluster of Excellence ct.qmat, Lehrstuhl für Technische Physik, Am Hubland, 97074 Würzburg, Germany. [4]Department of Physics and Astronomy, University of Southampton, Southampton SO17 1BJ, UK.
*Corresponding author. Email: p.ledingham@soton.ac.uk
†These authors contributed equally to this work.

facilitated by a high-finesse fiber-based optical cavity has been demonstrated (*38*). Last, dispersive delay of 879.7-nm QD light in a cryogenically cooled Nd^{3+}:YVO_4 crystal has been achieved using the atomic frequency comb protocol (*39*). However, storage and active retrieval of light from a QD single-photon source in an atomic quantum memory has not previously been demonstrated because of the challenge of having an on-demand memory that has high efficiency over a sufficiently large bandwidth and low enough noise. This feature of active retrieval, where the light is retrieved from the memory on-demand is a strict requirement for any quantum memory protocol for applications in a future quantum network.

In this work, we experimentally demonstrate the storage and active recall of deterministic telecom light emitted from a semiconductor QD single-photon source in a hot rubidium vapor quantum memory. To address the challenge of bandwidth matching between the source and memory, we use the ORCA memory protocol, which offers gigahertz-bandwidth storage and the lowest noise floor of any atomic ensemble–based quantum memory with less than 10^{-6} noise photons per pulse, and can store telecom-band light directly (*40*). The single photons are delivered by a metal–organic vapor-phase epitaxy (MOVPE)-grown InAs QD (*41*) that has been specifically designed and fabricated to emit close to the operation wavelength of the ORCA memory (1529.3 nm) with gigahertz bandwidth. Some additional spectral and temporal shaping are used to further condition the light to match the properties of the memory. To our knowledge, this is the first demonstration of storage and active retrieval of light from a QD single-photon source in an atomic quantum memory—a hybrid quantum light-matter interface—all while operating at a telecommunication wavelength.

RESULTS

The quantum memory is based on the ORCA protocol in rubidium vapor, where a strong control pulse detuned from the 780.2-nm Rb D2 line ($5S_{1/2}$-$5P_{3/2}$) by Δ dynamically induces the absorption of the QD photon at 1529.3 nm into the $4D_{5/2}$ excited state, as shown in Fig. 1A. The QD photon is then stored as a collective coherence between the ground and storage states. The ORCA memory protocol offers on-demand retrieval because the application of a second control pulse at a controllable later time actively maps this atomic coherence back to an optical field.

The single-photon source is based on InAs QDs grown on top of a jump-convex-inverse InGaAs metamorphic buffer (MMB) (see Fig. 1B) that enables emission in the telecom band (*41*). The QDs are grown inside a cavity formed by a bottom distributed Bragg reflector (DBR) composed of 23 AlAs/GaAs pairs and a top DBR of 4 SiO_2/TiO_2 pairs (see Materials and Methods). This planar cavity structure increases the QD light extraction, and the thickness is adapted for operation at 1529.3 nm. The QD is excited through quasi-resonant p-shell excitation using 3-ps laser pulses with a central wavelength of 1505 nm and a repetition rate of 80 MHz. The single photons are separated from the excitation laser using three bandpass filters with a 12-nm full width at half maximum (FWHM) bandwidth. A high-resolution spectrometer is used to identify a QD that emits light at precise wavelength of the ORCA quantum memory, as shown in Fig. 2A. The output of the QD single-photon source is measured using superconducting nanowire single-photon detectors (SNSPDs), and the recorded count rate is 4×10^5 s^{-1}. The second-order autocorrelation of the collected light is measured in a Hanbury Brown-Twiss setup and found to be $g^{(2)}(0) = 0.306 \pm 0.002$ (see Fig. 2B), which verifies nonclassicality and is consistent with a predominantly single-photon output.

The photons emitted by the QD have an exponentially decaying temporal intensity profile with a $1/e$ decay time of 0.85 ± 0.01 ns. With the Doppler-limited characteristic $1/e$ lifetime of the memory being 1.1 ns (*40*), there is a high probability of input photons in the retrieval window of the memory, as shown in Fig. 2C. To ensure that

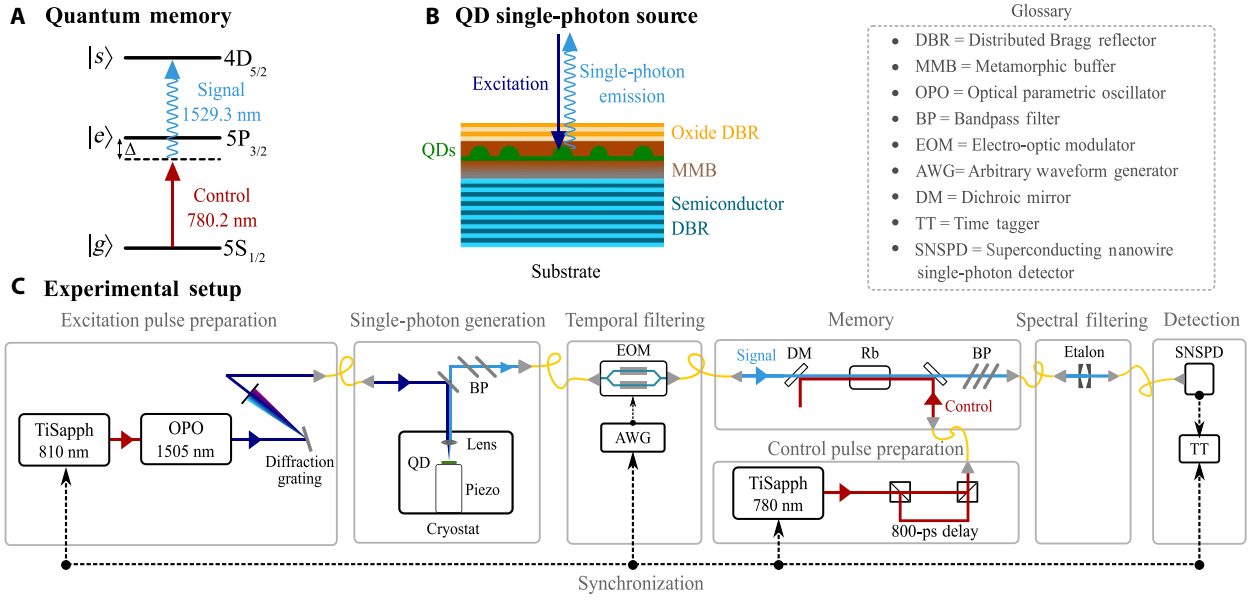

Fig. 1. Schematic of the experimental setup for the QD–quantum memory interface. (**A**) Energy level scheme for the telecom ORCA quantum memory protocol in rubidium vapor. (**B**) Scheme of the semiconductor QD sample with semiconductor bottom DBR, metamorphic buffer (MMB), and oxide top DBR. (**C**) Experimental setup of the hybrid interface to store photons from a QD single-photon source in a quantum memory.

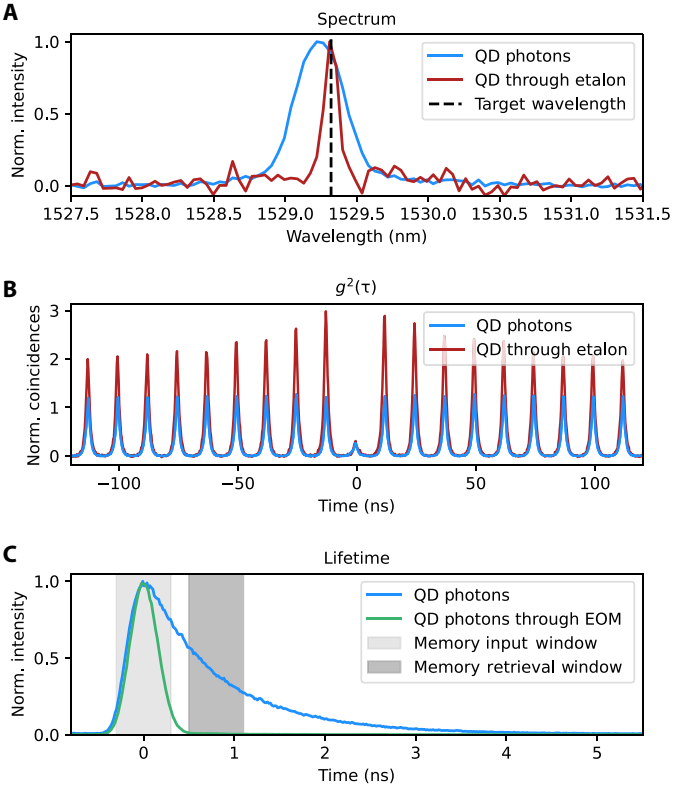

Fig. 2. Characterization of single-photon source. (**A**) Spectrum of photons from QD without (blue) and with (red) spectral filtering from the etalon, normalized to the maximum intensity. The dashed black line shows the target wavelength of the memory. (**B**) The second-order autocorrelation, $g^{(2)}(\tau)$, of photons from the QD without (blue) and with (red) the etalon. The data are normalized to the height of the Poissonian coincidence peaks at long time delays. The etalon introduces blinking that results in bunching (increased coincidences) at short time delays (see the Supplementary Materials). (**C**) Arrival time histogram of photons from the QD without (blue) and with (green) temporal filtering through the EOM, normalized to the maximum intensity. The shaded regions indicate the input and retrieval windows of the quantum memory, with a chosen storage time of 800 ps.

the input and retrieval signals are temporally well separated, we temporally filtered the single photons to a Gaussian temporal mode shape with an FWHM of 300 ps before being sent into the memory, as shown in Fig. 2C. This is achieved using an Electro-Optic Modulator (EOM) intensity modulator that is driven by an arbitrary waveform generator (AWG). A retrieval time of 800 ps is chosen, representing a trade-off between the memory lifetime and fractional delay.

The 1-GHz control pulse bandwidth determines the operational bandwidth of the quantum memory. The homogeneous linewidth of a single photon emitted from the QD is around 200 MHz as estimated from the lifetime in Fig. 2C. However, because of charge noise and spin noise in the system, the central frequency of emission is inhomogeneously broadened with an estimated FWHM of around 12 GHz (see the Supplementary Materials) (*23*, *42*). This spectral mismatch between the bandwidth of the memory and the total inhomogeneous bandwidth of the single-photon emission means that only a small proportion of the QD photons are on resonance with the memory, leading to a low memory efficiency (see the Supplementary Materials). To increase the observed memory efficiency, we spectrally filter the photons from the QD single-photon source using a Fabry-Perot etalon with a bandwidth of 1.12 ± 0.02 GHz, which selects the photons that are on resonance with the memory. The transmission of the broadened QD emission line through the etalon is around 3%. The spectrum of the QD photons filtered by the etalon is shown in Fig. 2A, and the corresponding $g^{(2)}$ measurement is shown in red in Fig. 2B from which we extract $g^{(2)}(0) = 0.325 \pm 0.008$. This $g^{(2)}$-measurement shows some blinking that originates from the spectral filtering of the emission line and therefore leads to artificial on-off times of the single-photon source (see the Supplementary Materials).

The loss introduced by both the temporal and spectral filtering substantially reduces the average photon number per pulse at the input to the memory. The detected count rate of the single photons transmitted through the entire setup when the control field is turned off is (203.4 ± 0.8) s^{-1} (for a full loss budget, see the Supplementary Materials). While the telecom ORCA quantum memory has the lowest noise floor of any atom-based quantum memory (*40*), a small amount of noise is generated by the interaction of the strong control pulses with the atomic ensemble (see the Supplementary Materials). The etalon is placed after the memory to further suppress this residual noise. The etalon therefore has two purposes: to spectrally filter the QD photons that did not interact with the memory and to filter any noise from the memory that is not at the signal frequency. The temporally filtered photons from the QD source are sent through the quantum memory, and the retrieved light on the output is filtered using the etalon and then sent to the detection setup. The full experimental setup is outlined in Fig. 1C, and details are given in Materials and Methods.

Figure 3 shows the arrival time histogram of photons at the output of the memory. When the control fields are present (red data), we see absorption of the photons into the memory. Active retrieval of the light is observed at the storage time of 800 ps due to the application of the read-out control pulse. To extract the efficiency of the storage and retrieval processes, we fit Gaussian wavepackets to the data—one Gaussian for the input signal and a sum of two Gaussians with a time separation for the transmitted (not stored in the memory) and retrieved signals (see the Supplementary Materials). From these fits, a read-in efficiency of $\eta_{in} = (49.3 \pm 0.4)\%$ and a total (internal) memory efficiency of $\eta_{tot} = (12.9 \pm 0.4)\%$ is extracted, considering a 500-ps integration window. The detected count rate of light retrieved from the memory in that integration window is (22 ± 1) s^{-1}. The gray data in Fig. 3 show the noise generated by the memory and detectors, measured with the control fields present and the input signal blocked. We note that the background count rate is the same regardless of whether the control field is turned on, which indicates that the noise is predominantly due to detector dark counts. We define the signal-to-noise ratio (SNR) as the ratio of signal light retrieved from the memory compared to the number of noise counts in the output window, and we measure SNR = 18.2 ± 0.6. This is the first demonstration of storage and on-demand recall of light from a solid-state single-photon source in an atomic quantum memory.

While the count rate in the retrieval window is insufficient to obtain statistically significant measurements of the $g^{(2)}(0)$ of the retrieved light within a reasonable experimental runtime, it can be inferred from the $g^{(2)}(0)$ of the input light and the SNR. We model the output of the memory as an incoherent admixture of the desired memory output with undesired detector dark count noise, treating both as independent fields with their own $g^{(2)}(0)$ values, with the mixing ratio given by the SNR, S (*29*, *43*, *44*). Under the assumption that

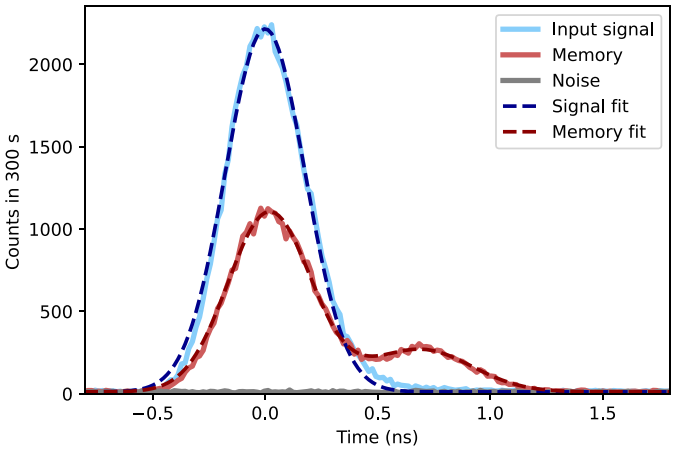

Fig. 3. Storage and retrieval of QD photons in ORCA memory. Arrival time histograms of QD photons through the ORCA memory for the input (blue), memory (red), and noise (gray) settings. The dashed lines are Gaussian fits to the data.

the $g^{(2)}_{\text{noise}}(0) = 1$, the predicted $g^{(2)}_{\text{out}}(0)$ of the output is given by (see the Supplementary Materials)

$$g^{(2)}_{\text{out}}(0) = \frac{1 + 2S + S^2 g^{(2)}_{\text{in}}(0)}{(1+S)^2} \quad (1)$$

With $g^{(2)}_{\text{in}}(0) = 0.325 \pm 0.008$ and $S = 18.2 \pm 0.6$, we predict $g^{(2)}_{\text{out}}(0) = 0.393 \pm 0.007$. This indicates that the noise level of this memory is sufficiently low to allow for storage and retrieval of quantum states of light well below the nonclassical threshold. This analysis does not take into account that the origin of $g^{(2)}_{\text{in}}(0) \neq 0$ could be, at least partially, due to insufficient suppression of the excitation laser that leads to additional unwanted photons in the input state that are distinguishable from the desired single-photon contribution. These unwanted photons would therefore not be on resonance with the quantum memory and would transmit straight through, and for that reason, the $g^{(2)}_{\text{out}}(0)$ of the light that is stored and then retrieved by the quantum memory could in fact be lower than the input state.

DISCUSSION

This first-of-its-kind demonstration of on-demand recall of QD light from an atomic memory is the first crucial step toward hybrid quantum light-matter interfaces for scalable quantum networks. To increase the overall throughput and efficiency of this interface, further improvements are needed to better match the temporal-spectral mode overlap between the source and memory.

To improve the spectral overlap, the inhomogeneous bandwidth of the solid-state emitters can be reduced using electrically contacted semiconductor devices that can decrease the charge noise (*10*, *45*). Alternatively, the bandwidth of the memory can be increased by increasing the control pulse bandwidth, although, to maintain low noise levels, it may be necessary to further detune from resonance requiring higher control pulse energies to maintain the same light-matter coupling efficiency. In either of these cases, the requirement of spectral filtering could be relaxed leading to substantially higher end-to-end efficiencies.

Temporal mode filtering of QD emission was a requirement in this current demonstration due to the 1-ns Doppler-limited memory lifetime. One means to overcome this limitation is to generate temporally shorter QD photons through optimized QD microstructures to further Purcell-enhance the emission. Alternatively, increasing the storage time would not only remove the need for lossy temporal filtering in this demonstration but also represent the ultimate goal of having a network-ready memory device. Removing the Doppler-dephasing limit is the first step toward this goal, and we outline several approaches. One can eliminate the Doppler effect by removing the atomic velocity with a magneto-optical trap. Challenges arise here in obtaining large-enough atom numbers for efficient light-matter interactions, as well as operating at a substantially reduced duty cycle limited by the loading and cooling steps of the trapping [e.g., 3% in (*46*)]. Instead of cooling and trapping, optical pumping can be used to tailor the velocity distribution of the atoms into a periodic structure to enact the atomic frequency comb protocol, i.e., a Doppler-rephasing approach, as demonstrated in alkali vapors in (*47*) by our team. This, in principle, allows for the ORCA coherence to be read out after any time multiple of the rephasing time (of order 10 ns is readily achievable) up to the excited-state lifetime but still remains to be demonstrated. As with the trapped atoms approach, sufficient optical depth and duty cycle will limit the operation.

A very promising approach is based on compensating for the Doppler dephasing with controlled dynamic AC-Stark shifts (*48*). The idea is that the collective ORCA coherence is continuously dressed with some auxiliary state with an (ideally) enhanced but opposite sensitivity to the Doppler shift. For our system, we identify the $8F_{7/2}$ excited state as a suitable candidate that connects to the storage state with a 792.7-nm optical field. To this end, we have implemented a proof-of-principle demonstration with our telecom ORCA memory (see the Supplementary Materials). Using weak coherent states of 0.1 photons per pulse, we observe $(8.69 \pm 0.03)\%$ total efficiency at a 2.3-ns storage time with the application of a 150-mW dressing field, representing a (279 ± 5)-fold increase in efficiency at that storage time, without a statistically significant increase in the measured noise. Much longer storage times up to the excited state lifetime could be achieved with higher power in the dressing field or appropriate temporal or frequency modulation of this field, as in (*48*). Further details are provided in the Supplementary Materials. To reach even longer storage times beyond the limit of the radiative lifetime of the storage state (here, ~90 ns), it would then be necessary to map the coherence to longer-lived states such as the hyperfine ground states using additional optical fields at a later time, where coherence times up to one second in warm atomic ensembles have been observed (*49*).

Last, the control pulses in the ORCA memory interaction act as time-nonstationary beamsplitters. First, this allows the interaction to be optimized to that of the input QD photon temporal mode, by temporal shaping of the control pulses, and, in principle, near-unit memory efficiency could be reached (*50*). Second, this enables temporal-spectral mode filtering and conversion (*6*), a capability that is out of reach for passive slow light–type interactions or fiber loop–based memories. The memory acts as a coherent mode filter, and, therefore, the indistinguishability of photons retrieved from the memory is predicted to be higher than the input (*6*). Furthermore, multiple quantum memories could be used to render the output of several QD photon sources to be indistinguishable by retrieving the photons into the same temporal-spectral mode, which would overcome a key challenge in the fabrication of many identical single-photon sources.

In conclusion, we have demonstrated the storage and on-demand retrieval of light emitted from a semiconductor QD in a rubidium vapor–based quantum memory, with operation in the low-loss telecommunication bands. This represents a key step toward the goal of an efficient hybrid interface between solid-state single-photon sources and atomic quantum memories, pivotal for developing future quantum network–ready devices.

MATERIALS AND METHODS

Experimental design

QD single-photon source fabrication

The QD sample structure follows the thin-film InGaAs MMB structure introduced by Sittig *et al.* (*41*). The MOVPE-grown sample features 23 AlAs/GaAs DBR pairs on top of the GaAs wafer substrate, followed by the jump convex–inverse InGaAs MMB. The nonlinear variation of In content simultaneously allows for sufficient strain reduction, a smooth surface, and a low MMB thickness. The MMB changes the lattice constant, so the self-assembled InAs QDs emit at around 1550 ± 75 nm. The thin MMB and the InGaAs capping layer form a λ-cavity around the QDs to benefit emission at the desired 1529.3 nm. The upper part of the sample consists of an oxide top DBR of four pairs of SiO_2/TiO_2 with a nominal thickness of 268 nm/168 nm and a 20-nm cap of SiO_2, to protect the surface, which was fabricated using plasma-enhanced sputter deposition. The planar cavity was designed with a strong asymmetry in the top DBR and bottom DBR reflectivities, such that the light will be guided predominantly upward. The bottom DBR has a calculated reflectivity of 99.2%, whereas the top DBR has a calculated reflectivity of 97.2%. To achieve a cavity at around 1529 nm, the thicknesses of the InGaAs MMB as well as the capping layer and the DBR layers have been decreased to shift the cavity to the lower desired wavelength.

QD single-photon source operation

The QD sample is placed inside a low-vibration closed-cycle cryostat (Attocube attoDRY800) and cooled to 4 K. The sample is mounted on top of a piezo stack that allows for precision positioning along three axes. An objective lens with a focal length of 3.1 mm (Thorlabs) and a numerical aperture of 0.68 is mounted inside the cryostat directly above the QD sample, which focuses the excitation laser to a spot size of ~2 μm on the top surface of the sample. The pulses for exciting the QD are generated from an optical parametric oscillator (OPO) that frequency converts pulses from a titanium:sapphire (Ti:Sapph) laser at 810 nm to around 1505 nm using a nonlinear optical crystal. The output pulses of the OPO are around 200 fs in duration. We spectrally filter these pulses using a diffraction grating and a pinhole to narrow the spectrum to 0.9 nm or a pulse duration of 3 ps. The emission from the sample is separated from the excitation laser using three 12-nm FWHM bandpass filters (Thorlabs), each of which have a transmission of 95% at 1529 nm and a suppression of approximately 10^5 at 1505 nm. The emitted light is coupled into a single-mode fiber and sent to a spectrometer with a resolution of 5.8 GHz per pixel and detected using a InGaAs charge-coupled device camera (Oxford Instruments Andor iDus). The wavelength of the QD emission is compared to the target wavelength of the quantum memory. We measure the count rate of the single-photon source on an SNSPD, which has an efficiency of $\eta_{detector} = 0.80$. To measure the single-photon purity of the collected light, we use a 50:50 fiber beam splitter and send both outputs of the beam splitter to a SNSPD. We record the correlations between the two detectors using a time tagger (TT; Swabian Instruments) to perform a second-order autocorrelation. From the correlation histogram, we can extract $g^{(2)}(0)$ from the ratio of the coincidence peak at zero time delay compared to the Poissonian level at long time delays (see the Supplementary Materials). We measure the temporal profile of the photons by performing a coincidence measurement between the SNSPD and the trigger from the OPO laser using the time tagger. The temporal profile of the photons is quite long compared to the maximum storage time of the quantum memory. We temporally filter the collected light using an EOM intensity modulator (iXblue), which has a continuous wave transmission of 45% and an extinction ratio of 20 dB. The EOM is driven by an radio frequency signal from an AWG (Tektronix). The trigger signal from the OPO is used as both an 80-MHz clock input and a trigger signal for the AWG, so that the intensity modulation is synchronized with the single-photon generation. The AWG outputs a Gaussian radio frequency signal with an FWHM of 300 ps. The time-filtered temporal profile of the photons is shown in Fig. 2C.

Quantum memory

The quantum memory is based on the telecom ORCA protocol in an ensemble of warm rubidium atoms (*40*). The ORCA memory uses three atomic energy levels, $|g\rangle$, $|e\rangle$, and $|s\rangle$ in a ladder configuration (see Fig. 1A). Two counterpropagating fields are both detuned from the intermediate transitions $|g\rangle \rightarrow |e\rangle$ and $|e\rangle \rightarrow |s\rangle$ by Δ but are in two-photon resonance with the $|g\rangle \rightarrow |s\rangle$ transition. The strong control field maps the incoming signal onto a coherence between the ground and storage states ($|g\rangle$ and $|s\rangle$). On application of a second control pulse at a later time, the atomic coherence is mapped back to an optical field, and the signal is retrieved from the memory. The implementation of the telecom ORCA memory uses an 8-cm-long cell of rubidium atoms that is warmed up to around 120°C, generating an optical depth of around 8500. The control pulses that drive the memory are generated from a mode-locked Ti:Sapph laser, which is synchronized to the OPO that excites the QD via a Lock-to-Clock module (Spectra Physics). An unbalanced Mach-Zehnder interferometer is used to generate two pulses separated by 800 ps to act as the read-in and read-out pulses of the memory. The read-in pulses have an energy of 0.4 nJ, and the read-out pulses have an energy of 4 nJ. The frequency of the control pulses is monitored using a high finesse wavemeter and is set to be 6 GHz red-detuned from the $|g\rangle \rightarrow |e\rangle$ transition. The single photons and control pulses travel counterpropagating through the vapor cell, and the two fields are combined and separated using dichroic mirrors (Semrock) that transmit 1529-nm light and reflect 780-nm light. The control pulses (single photons) are focused to a beam waist diameter of 250 μm (220 μm) at the center of the vapor cell, respectively. The single photons that are transmitted or stored/retrieved from the memory are coupled into a single-mode fiber, and a series of long-pass and band-pass filters (Thorlabs/Semrock) before the fiber is used to suppress the control field by 14 orders of magnitude. More details about the experimental setup of the memory are given in (*40*).

The light that is collected at the output of the memory is detected using an SNSPD with 70-ps timing jitter (PhotonSpot). A time tagger (Swabian Instruments) is used to generate correlation histograms between the single-photon detector and the trigger of the OPO laser. An arrival time histogram is measured for three settings: (i) "Signal," input photons only; (ii) "Memory," input photons and control pulses; (iii) "Noise," control pulses only. To minimize the effect of any slow drifts in the experiment, data are recorded for each of the three settings for 60 s in a repeated cyclic

manner, until the total cumulative counts are sufficient to extract the efficiency and SNR.

Supplementary Materials

This PDF file includes:

Supplementary Text
Figs. S1 to S8
Table S1
References

REFERENCES AND NOTES

1. K. Hammerer, A. S. Sørensen, E. S. Polzik, Quantum interface between light and atomic ensembles. *Rev. Mod. Phys.* **82**, 1041–1093 (2010).
2. K. Heshami, D. G. England, P. C. Humphreys, P. J. Bustard, V. M. Acosta, J. Nunn, B. J. Sussman, Quantum memories: Emerging applications and recent advances. *J. Mod. Opt.* **63**, 2005–2028 (2016).
3. A. G. Radnaev, Y. O. Dudin, R. Zhao, H. H. Jen, S. D. Jenkins, A. Kuzmich, T. A. B. Kennedy, A quantum memory with telecom-wavelength conversion. *Nat. Phys.* **6**, 894–899 (2010).
4. B. M. Sparkes, M. Hosseini, C. Cairns, D. Higginbottom, G. T. Campbell, P. K. Lam, B. C. Buchler, Precision spectral manipulation: A demonstration using a coherent optical memory. *Phys. Rev. X* **2**, 021011 (2012).
5. C. Liu, T. Tao, P.-Y. Li, X. Liu, X.-Y. Zhu, Z.-Q. Zhou, C.-F. Li, G.-C. Guo, Towards entanglement distillation between atomic ensembles using high-fidelity spin operations. *Commun. Phys.* **5**, 67 (2022).
6. S. Gao, O. Lazo-Arjona, B. Brecht, K. T. Kaczmarek, S. E. Thomas, J. Nunn, P. M. Ledingham, D. J. Saunders, I. A. Walmsley, Optimal coherent filtering for single noisy photons. *Phys. Rev. Lett.* **123**, 213604 (2019).
7. N. Somaschi, V. Giesz, L. De Santis, J. C. Loredo, M. P. Almeida, G. Hornecker, S. L. Portalupi, T. Grange, C. Anton, J. Demory, C. Gomez, I. Sagnes, N. D. Lanzillotti-Kimura, A. Lemaitre, A. Auffeves, A. G. White, L. Lanco, P. Senellart, Near-optimal single-photon sources in the solid state. *Nat. Photon.* **10**, 340–345 (2016).
8. N. Tomm, A. Javadi, N. O. Antoniadis, D. Najer, M. C. Löbl, A. R. Korsch, R. Schott, S. R. Valentin, A. D. Wieck, A. Ludwig, R. J. Warburton, A bright and fast source of coherent single photons. *Nat. Nanotechnol.* **16**, 399–403 (2021).
9. D. Huber, M. Reindl, Y. Huo, H. Huang, J. S. Wildmann, O. G. Schmidt, A. Rastelli, R. Trotta, Highly indistinguishable and strongly entangled photons from symmetric GaAs quantum dots. *Nat. Commun.* **8**, 15506 (2017).
10. L. Zhai, M. C. Löbl, G. N. Nguyen, J. Ritzmann, A. Javadi, C. Spinnler, A. D. Wieck, A. Ludwig, R. J. Warburton, Low-noise GaAs quantum dots for quantum photonics. *Nat. Commun.* **11**, 4745 (2020).
11. T. van Leent, M. Bock, R. Garthoff, K. Redeker, W. Zhang, T. Bauer, W. Rosenfeld, C. Becher, H. Weinfurter, Long-distance distribution of atom-photon entanglement at telecom wavelength. *Phys. Rev. Lett.* **124**, 010510 (2020).
12. C. L. Morrison, M. Rambach, Z. Xian Koong, F. Graffitti, F. Thorburn, A. K. Kar, Y. Ma, S.-I. Park, J. Dong Song, N. G. Stoltz, D. Bouwmeester, A. Fedrizzi, B. D. Gerardot, A bright source of telecom single photons based on quantum frequency conversion. *Appl. Phys. Lett.* **118**, 174003 (2021).
13. C. Clausen, I. Usmani, F. Bussieres, N. Sangouard, M. Afzelius, H. de Riedmatten, N. Gisin, Quantum storage of photonic entanglement in a crystal. *Nature* **469**, 508–511 (2011).
14. K. T. Kaczmarek, P. M. Ledingham, B. Brecht, S. E. Thomas, G. S. Thekkadath, O. Lazo-Arjona, J. H. D. Munns, E. Poem, A. Feizpour, D. J. Saunders, J. Nunn, I. A. Walmsley, High-speed noise-free optical quantum memory. *Phys. Rev. A* **97**, 042316 (2018).
15. A. Seri, A. Lenhard, D. Rieländer, M. Gundogan, P. M. Ledingham, M. Mazzera, H. de Riedmatten, Quantum correlations between single telecom photons and a multimode on-demand solid-state quantum memory. *Phys. Rev. X* **7**, 021028 (2017).
16. G. Buser, R. Mottola, B. Cotting, J. Wolters, P. Treutlein, Single-photon storage in a ground-state vapor cell quantum memory. *PRX Quantum* **3**, 020349 (2022).
17. A. J. Bennett, M. A. Pooley, R. M. Stevenson, M. B. Ward, R. B. Patel, A. Boyer de la Giroday, N. Sköld, I. Farrer, C. A. Nicoll, D. A. Ritchie, A. J. Shields, Electric-field-induced coherent coupling of the exciton states in a single quantum dot. *Nat. Phys.* **6**, 947–950 (2010).
18. N. Akopian, L. Wang, A. Rastelli, O. G. Schmidt, V. Zwiller, Hybrid semiconductor-atomic interface: Slowing down single photons from a quantum dot. *Nat. Photonics* **5**, 230–233 (2011).
19. C. E. Kuklewicz, R. N. E. Malein, P. M. Petroff, B. D. Gerardot, Electro-elastic tuning of single particles in individual self-assembled quantum dots. *Nano Lett.* **12**, 3761–3765 (2012).
20. K. D. Jöns, R. Hafenbrak, P. Atkinson, A. Rastelli, O. G. Schmidt, P. Michler, Quantum state tomography measurements on strain-tuned $In_xGa_{1-x}As$/GaAs quantum dots. *Phys. Status Solidi B* **249**, 697–701 (2012).
21. R. Trotta, E. Zallo, C. Ortix, P. Atkinson, J. D. Plumhof, J. Van Den Brink, A. Rastelli, O. G. Schmidt, Universal recovery of the energy-level degeneracy of bright excitons in InGaAs quantum dots without a structure symmetry. *Phys. Rev. Lett.* **109**, 147401 (2012).
22. A. Kiraz, P. Michler, C. Becher, B. Gayral, A. Imamoglu, E. H. Lidong Zhang, W. V. Schoenfeld, P. M. Petroff, Cavity-quantum electrodynamics using a single InAs quantum dot in a microdisk structure. *Appl. Phys. Lett.* **78**, 3932–3934 (2001).
23. A. V. Kuhlmann, J. Houel, A. Ludwig, L. Greuter, D. Reuter, A. D. Wieck, M. Poggio, R. J. Warburton, Charge noise and spin noise in a semiconductor quantum device. *Nat. Phys.* **9**, 570–575 (2013).
24. M. P. Hedges, J. J. Longdell, Y. Li, M. J. Sellars, Efficient quantum memory for light. *Nature* **465**, 1052–1056 (2010).
25. Y.-W. Cho, G. T. Campbell, J. L. Everett, J. Bernu, D. B. Higginbottom, M. T. Cao, J. Geng, N. P. Robins, P. K. Lam, B. C. Buchler, Highly efficient optical quantum memory with long coherence time in cold atoms. *Optica* **3**, 100–107 (2016).
26. P. Vernaz-Gris, K. Huang, M. Cao, A. S. Sheremet, J. Laurat, Highly-efficient quantum memory for polarization qubits in a spatially-multiplexed cold atomic ensemble. *Nat. Commun.* **9**, 363 (2018).
27. J. Wolters, G. Buser, A. Horsley, L. Beguin, A. Jöckel, J.-P. Jahn, R. J. Warburton, P. Treutlein, Simple atomic quantum memory suitable for semiconductor quantum dot single photons. *Phys. Rev. Lett.* **119**, 060502 (2017).
28. R. Finkelstein, E. Poem, O. Michel, O. Lahad, O. Firstenberg, Fast, noise-free memory for photon synchronization at room temperature. *Sci. Adv.* **4**, eaap8598 (2018).
29. P. S. Michelberger, T. F. M. Champion, M. R. Sprague, K. T. Kaczmarek, M. Barbieri, X. M. Jin, D. G. England, W. S. Kolthammer, D. J. Saunders, J. Nunn, I. A. Walmsley, Interfacing GHz-bandwidth heralded single photons with a warm vapour Raman memory. *New J. Phys.* **17**, 043006 (2015).
30. H. Huang, R. Trotta, Y. Huo, T. Lettner, J. S. Wildmann, J. Martin-Sanchez, D. Huber, M. Reindl, J. Zhang, E. Zallo, O. G. Schmidt, A. Rastelli, Electrically-pumped wavelength-tunable GaAs quantum dots interfaced with rubidium atoms. *ACS Photonics* **4**, 868–872 (2017).
31. J. S. Wildmann, R. Trotta, J. Martin-Sanchez, E. Zallo, M. O'Steen, O. G. Schmidt, A. Rastelli, Atomic clouds as spectrally selective and tunable delay lines for single photons from quantum dots. *Phys. Rev. B* **92**, 235306 (2015).
32. R. Trotta, J. Martin-Sanchez, J. S. Wildmann, G. Piredda, M. Reindl, C. Schimpf, E. Zallo, S. Stroj, J. Edlinger, A. Rastelli, Wavelength-tunable sources of entangled photons interfaced with atomic vapours. *Nat. Commun.* **7**, 10375 (2016).
33. S. L. Portalupi, M. Widmann, C. Nawrath, M. Jetter, P. Michler, J. Wrachtrup, I. Gerhardt, Simultaneous Faraday filtering of the Mollow triplet sidebands with the Cs-D_1 clock transition. *Nat. Commun.* **7**, 13632 (2016).
34. H. Vural, S. L. Portalupi, J. Maisch, S. Kern, J. H. Weber, M. Jetter, J. Wrachtrup, R. Löw, I. Gerhardt, P. Michler, Two-photon interference in an atom–quantum dot hybrid system. *Optica* **5**, 367 (2018).
35. T. Kroh, J. Wolters, A. Ahlrichs, A. W. Schell, A. Thoma, S. Reitzenstein, J. S. Wildmann, E. Zallo, R. Trotta, A. Rastelli, O. G. Schmidt, O. Benson, Slow and fast single photons from a quantum dot interacting with the excited state hyperfine structure of the Cesium D1-line. *Sci. Rep.* **9**, 13728 (2019).
36. J. Maisch, H. Vural, M. Jetter, P. Michler, I. Gerhardt, S. L. Portalupi, Controllable delay and polarization routing of single photons. *Adv. Quantum Technol.* **3**, 1900057 (2020).
37. G.-D. Cui, L. Schweickert, K. D. Jöns, M. Namazi, T. Lettner, K. D. Zeuner, L. Scavuzzo Montana, S. F. C. da Silva, M. Reindl, H. Huang, R. Trotta, A. Rastelli, V. Zwiller, E. Figueroa, Coherent quantum interconnection between on-demand quantum dot single photons and a resonant atomic quantum memory. arXiv:2301.10326 [quant-ph] (24 January 2023).
38. H. M. Meyer, R. Stockill, M. Steiner, C. Le Gall, C. Matthiesen, E. Clarke, A. Ludwig, J. Reichel, M. Atature, M. K¨ohl., Direct photonic coupling of a semiconductor quantum dot and a trapped ion. *Phys. Rev. Lett.* **114**, 123001 (2015).
39. J.-S. Tang, Z.-Q. Zhou, Y.-T. Wang, Y.-L. Li, X. Liu, Y.-L. Hua, Y. Zou, S. Wang, D.-Y. He, G. Chen, Y.-N. Sun, Y. Yu, M.-F. Li, G.-W. Zha, H.-Q. Ni, Z.-C. Niu, C.-F. Li, G.-C. Guo, Storage of multiple single-photon pulses emitted from a quantum dot in a solid-state quantum memory. *Nat. Commun.* **6**, 8652 (2015).
40. S. E. Thomas, S. Sagona-Stophel, Z. Schofield, I. A. Walmsley, P. M. Ledingham, Single-photon-compatible telecommunications-band quantum memory in a hot atomic gas. *Phys. Rev. Appl.* **19**, L031005 (2023).
41. R. Sittig, C. Nawrath, S. Kolatschek, S. Bauer, R. Schaber, J. Huang, P. Vijayan, P. Pruy, S. L. Portalupi, M. Jetter, P. Michler, Thin-film InGaAs metamorphic buffer for telecom C-band InAs quantum dots and optical resonators on GaAs platform. *Nanophotonics* **11**, 1109–1116 (2022).
42. C. Nawrath, H. Vural, J. Fischer, R. Schaber, S. L. Portalupi, M. Jetter, P. Michler, Resonance fluorescence of single In(Ga)As quantum dots emitting in the telecom C-band. *Appl. Phys. Lett.* **118**, 244002 (2021).
43. E. A. Goldschmidt, F. Piacentini, I. R. Berchera, S. V. Polyakov, S. Peters, S. Kuck, G. Brida, I. P. Degiovanni, A. Migdall, M. Genovese, Mode reconstruction of a light field by multiphoton statistics. *Phys. Rev. A* **88**, 013822 (2013).

44. S. E. Thomas, T. M. Hird, J. H. D. Munns, B. Brecht, D. J. Saunders, J. Nunn, I. A. Walmsley, P. M. Ledingham, Raman quantum memory with built-in suppression of four-wave-mixing noise. *Phys. Rev. A* **100**, 033801 (2019).
45. A. K. Nowak, S. L. Portalupi, V. Giesz, O. Gazzano, C. Dal Savio, P.-F. Braun, K. Karrai, C. Arnold, L. Lanco, I. Sagnes, A. Lema ̂ıtre, P. Senellart, Deterministic and electrically tunable bright single-photon source. *Nat. Commun.* **5**, 3240 (2014).
46. Y. Wang, J. Li, S. Zhang, K. Su, Y. Zhou, K. Liao, S. Du, H. Yan, S.-L. Zhu, Efficient quantum memory for single-photon polarization qubits. *Nat. Photonics* **13**, 346–351 (2019).
47. D. Main, T. M. Hird, S. Gao, E. Oguz, D. J. Saunders, I. A. Walmsley, P. M. Ledingham, Preparing narrow velocity distributions for quantum memories in room-temperature alkali-metal vapors. *Phys. Rev. A* **103**, 043105 (2021).
48. R. Finkelstein, O. Lahad, I. Cohen, O. Davidson, S. Kiriati, E. Poem, O. Firstenberg, Continuous protection of a collective state from inhomogeneous dephasing. *Phys. Rev. X* **11**, 011008 (2021).
49. O. Katz, O. Firstenberg, Light storage for one second in room-temperature alkali vapor. *Nat. Commun.* **9**, 2074 (2018).
50. J. Guo, X. Feng, P. Yang, Z. Yu, L. Q. Chen, C.-H. Yuan, W. Zhang, High-performance Raman quantum memory with optimal control in room temperature atoms. *Nat. Commun.* **10**, 148 (2019).
51. G. Björk, H. Heitmann, Y. Yamamoto, Spontaneous-emission coupling factor and mode characteristics of planar dielectric microcavity lasers. *Phys. Rev. A* **47**, 4451–4463 (1993).
52. C. Nawrath, F. Olbrich, M. Paul, S. L. Portalupi, M. Jetter, P. Michler, Coherence and indistinguishability of highly pure single photons from non-resonantly and resonantly excited telecom C-band quantum dots. *Appl. Phys. Lett.* **115**, 023103 (2019).
53. J. Minar, N. Sangouard, M. Afzelius, H. de Riedmatten, N. Gisin, Spin-wave storage using chirped control fields in atomic frequency comb-based quantum memory. *Phys. Rev. A* **82**, 042309 (2010).
54. M. Namazi, C. Kupchak, B. Jordaan, R. Shahrokhshahi, E. Figueroa, Ultralow-noise room-temperature quantum memory for polarization qubits. *Phys. Rev. Appl.* **8**, 034023 (2017).
55. M. Zugenmaier, K. B. Dideriksen, A. S. Sørensen, B. Albrecht, E. S. Polzik, Long-lived non-classical correlations towards quantum communication at room temperature. *Commun. Phys.* **1**, 76 (2018).

Acknowledgments: We thank M. Wagenbrenner for reliable layer deposition for the dielectric DBR. **Funding:** This work was supported by: Horizon 2020 research and innovation program grant agreement no. 899814 QUROPE (to M.J., P.M., I.A.W., S.L.P., and P.M.L.), Horizon 2020 research and innovation program grant agreement no. 899587 Stormytune (to P.M.L. and I.A.W.), and Engineering and Physical Sciences Research Council via the Quantum Computing and Simulation Hub (grant no. T001062) (to I.A.W.). We gratefully acknowledge the funding by the German Federal Ministry of Education and Research (BMBF) via the project QR.X (no. 16KISQ013) (to S.H. and P.M.). S.E.T. acknowledges an Imperial College Research Fellowship. P.M.L. acknowledges support from UK Research and Innovation (Future Leaders Fellowship, grant reference MR/V023845/1). T.H.-L. acknowledges support by the BMBF (Qecs–grant no. 13N16272). **Author contributions:** Conceptualization: P.M., I.A.W., S.L.P., and P.M.L.. Investigation: S.E.T., L.W., P.B., I.M.d.B.W., M.J.R., S.S.-S., and P.M.L. Resources: L.W., R.J., C.N., R.S., T.H.-L., and S.H. Supervision: P.M., I.A.W., S.L.P., and P.M.L.. Writing—original draft: S.E.T. Writing—review and editing: All authors. **Competing interests:** I.A.W. is a cofounder and chair of ORCA Computing. The authors declare that they have no other competing interests. **Data and materials availability:** All data needed to evaluate the conclusions in the paper are present in the paper and/or the Supplementary Materials.

Submitted 17 May 2023
Accepted 12 March 2024
Published 12 April 2024
10.1126/sciadv.adi7346